Time- and Polarization-Resolved Photoluminescence of Individual Semicrystalline Polythiophene (P3HT) Nanoparticles

ARTICLE *in* JOURNAL OF PHYSICAL CHEMISTRY LETTERS · AUGUST 2011

Impact Factor: 7.46 · DOI: 10.1021/jz200958x

7 AUTHORS, INCLUDING:

Joelle A Labastide
University of Massachusetts Amherst
12 PUBLICATIONS **150** CITATIONS
SEE PROFILE

Mina Baghgar
15 PUBLICATIONS **154** CITATIONS
SEE PROFILE

Dhandapani Venkataraman
University of Massachusetts Amherst
114 PUBLICATIONS **4,364** CITATIONS
SEE PROFILE

Michael D Barnes
University of Massachusetts Amherst
147 PUBLICATIONS **2,325** CITATIONS
SEE PROFILE

THE JOURNAL OF PHYSICAL CHEMISTRY C

Article

pubs.acs.org/JPCC

Time- and Polarization-Resolved Photoluminescence Decay from Isolated Polythiophene (P3HT) Nanofibers

Joelle A. Labastide,[†] Mina Baghgar,[‡] Aidan McKenna,[§] and Michael D. Barnes*[,†,‡]

[†]Department of Chemistry, [‡]Department of Physics, and [§]Department of Chemical Engineering, University of Massachusetts—Amherst, Amherst, Massachusetts 01003, United States

ABSTRACT: Isolated nanofibers present unique opportunities to investigate excitonic processes and dynamics in a confined crystalline geometry, where structural order in the transverse (intrachain) and longitudinal (interchain) directions can be tuned by polymer molecular weight, regioregularity, and solvent processing conditions. We report on time- and polarization-resolved photoluminescence (TRPL) studies from isolated crystalline P3HT nanofibers (also known as nanowires), which reveal a highly reproducible short-time decay behavior, appearing as an amplified spontaneous emission process (biexciton annihilation) as signaled by a quadratic excitation power dependence in amplitude and decay rate. In the long-time (5−100 ns) regime, we observed a power-law decay in the photoluminescence similar to that seen in thin films and nanoparticles; however, for certain nanofiber families (prepared from *p*-xylene) we observe an extremely long-lived PL component which we postulate arises from deeply trapped carriers in chain packing faults within the NF. Finally, we probe depolarization dynamics in individual nanofibers using polarization-resolved TRPL measurements in which both arrival time and (parallel/perpendicular) polarization state relative to the nanofiber axis are resolved, delineating the different dynamics associated with intra- and interchain excitons.

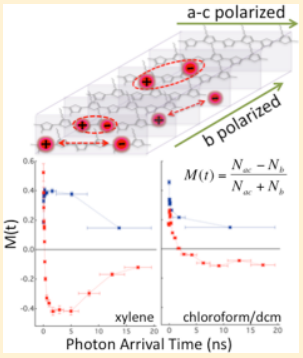

1. INTRODUCTION

The search for efficient photovoltaic devices based on cheap, solution-processable semiconducting polymers has spurred a massive research effort on the development of new materials and strategies for controlled nanoscale morphologies of OPV active layers.[1−8] Much of this new research has focused on poly(alkylthiophene) (e.g., poly(3-hexylthiopehene), P3HT)-based systems, and a wealth of new information on photophysical processes is emerging from a variety of thin-film[9−11] and nanoparticle[12,13] photoluminescence measurements. One of the key limitations, however, is the significant nanoscale structural heterogeneity in bulk structures, deriving from a combination of P3HT molecular weight and regioregularity effects, as well as processing conditions, making a direct connection between polymer morphology and photophysics difficult.[14−17] Quasi-two-dimensional crystalline nanofibers (NFs) of P3HT, formed by assembly of lamellar sheets via $\pi-\pi$ interactions, present an interesting model system to study the connection between polymer structure and photophysics.[18−21] However, only very recently have experimental techniques evolved to probe photoluminescence properties of isolated nanofibers.[22−24]

In this paper, we present results of time- and polarization-resolved photoluminescence measurements on isolated NFs designed to investigate the role of regioregularity, molecular weight, and solvent processing on inter- and intrachain coupling and the fate of photogenerated charges within the nanofiber. We identified three distinct time regimes in the photoluminescence decay that can be assigned to different processes within the nanofiber: In the long (>5 ns) time regime, the PL decay behavior can be understood within a model similar to that proposed by Silva[25] and Rumbles,[26] where exciton dissociation followed by polaron diffusion and subsequent trapping or recombination leads to a modified power law decay. In the short-time regime, we show that the fastest decay component derives from a cooperative biexciton decay process, in which both the amplitude and decay rate scale approximately quadratically with excitation intensity. Finally, polarization-resolved PL decay in the nanofiber frame gives interesting new insights into intra- and interchain coupling in isolated nanofibers and how that coupling can be modified by solvent processing conditions.

Poly(alkylthiophene)s—in particular, regioregular (rr) poly(3-hexylthiophene) (P3HT)—represent perhaps the most widely studied hole-transporting polymer for organic energy harvesting applications.[27] It is commonly accepted that the primary photoexcitations in P3HT are singlet Frenkel excitons initially delocalized over 15−20 monomer units.[10] As shown by transient absorption experiments,[10,28] photoproduced excitons in isolated single P3HT chains undergo a torsional relaxation (self-trapping) on an ultrafast time scale of ≤100 fs, followed by singlet exciton recombination with a characteristic time scale of ≈600 ps. In aggregated P3HT, charge separation followed by carrier diffusion and recombination via tunneling is associated with long-time (10−100 ns in thin films) photoluminescence decay.[11,25,26,29] Photophysical behavior in crystalline P3HT is intimately connected to regioregularity and molecular weight,[17,30−34] both of which control intra- and interchain

Received: August 27, 2012
Revised: October 2, 2012
Published: October 11, 2012

structural coherence lengths. Increasing the regioregularity of the polymer allows for better alignment of hexyl side chains during crystallization, which can also affect planarity of the polymer chains within the nanofiber and is manifest in differences in excitonic (H or J type) coupling.[35−37]

Figure 1 shows a schematic of the dynamic model for photoexcitations in P3HT in which excitons can recombine

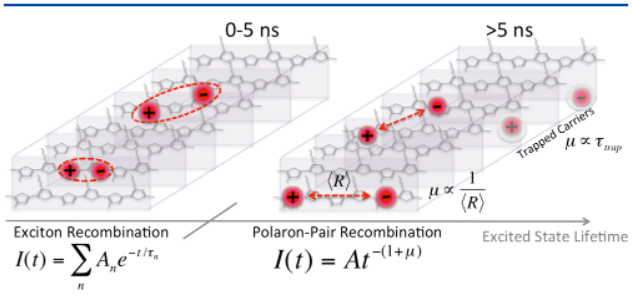

Figure 1. Schematic model for radiative recombination in crystalline P3HT. Direct recombination of relaxed (self-trapped) excitons follow distributed exponential kinetics in the short-time regime. Exciton dissociation followed by recombination (via tunneling) follows a power law decay. Subpower law decay ($I(t) \approx$ constant) appears for long-lived trapped carriers.

directly or dissociate. Upon dissociation, the polaron pair can undergo diffusion followed by recombination via tunneling[9] or become trapped and recombine after being released.[26,38] Direct exciton recombination results in short time relaxation dynamics (i.e., photon detection events occurring in the first 3 ns) that follow exponential rate laws; in semicrystalline P3HT, two fluorescence lifetimes of ∼180 ps (τ_1) and 1.5 ns (τ_2) are observed. In the long-time regime (10−100 ns), PL decay is governed by polaron pair recombination via tunneling and follows a power law rate equation, $I(t) = At^{-(1+\mu)}$.[9] In this model, the parameter μ is a dimensionless ratio of tunneling width to mean electron−hole radius. Recently, this model has been generalized to accommodate long-lived trapped charges, which account for sub-power law behavior where $I(t) \approx$ constant.[26,38]

Crystalline P3HT nanofibers represent an interesting model system with a well-defined chain packing structure that has been characterized extensively by X-ray diffraction and high-resolution electron microscopy.[19,20,39−42] Assembled in solution by addition of poor solvents for P3HT, these quasi-two-dimensional nanostructures are particularly interesting in the context of organic photovoltaic applications because of their potential to enable long-range charge transport. In a poor solvent, elongated P3HT chains assemble via side-chain interactions into lamellar sheets; these lamellae assemble along the **b** (010 crystallographic axis) direction via van der Waals interactions to form nanofibers that range from ≈100 nm to tens of micrometers in length.[20,42] The separation distance between lamellar sheets, as measured by X-ray diffraction and high-resolution transmission electron microscopy, is essentially the van der Waals contact diameter ≈3.8 Å, and the center-to-center distance between individual chains in the transverse **a**−**c** (100 and 001 crystallographic axes) direction depends on the degree of side-chain interdigitation, typically ≈1.5 nm. Knowledge of the basic NF assembly structure enables photophysical properties such as charge photogeneration, separation, and transport to be correlated directly with inter- and intrachain coupling.[24,41,43] Recent work by Moule[20] and Brinkmann[42] have shown how the local microstructure of individual nanofibers can be controlled to a certain extent by solvent interactions and polymer structure (regioregularity and molecular weight).

In recent single-nanofiber experiments by Gray and co-workers, wavelength-resolved photoluminescence in very small (<1 μm length) isolated NFs showed spectroscopic signatures of (intrachain) J-type excitonic coupling, evidenced by strong 0−0 luminescence with small (<90 meV) Stokes shift with respect to the solution phase origin.[23] Recently, work in our group on extended (>3 μm length) nanofibers revealed spectroscopic signatures of both J- and H-type coupling, as signaled by the presence of multiple vibronic replicas offset by ≈80 meV.[24] While it has been commonly thought that only one type of excitonic coupling would dominate (H or J), recent work by Yamagata and Spano suggests that hybrid H/J coupling—sensitive to the precise cofacial alignment of thiophene rings—is possible in these systems.[43] Thus, isolated nanofibers present unique opportunities to investigate excitonic processes and dynamics in a confined crystalline geometry, where inter- and intrachain couplings can be tuned by polymer molecular weight, regioregularity, and solvent processing conditions.

2. EXPERIMENTAL SECTION

Two main families of P3HT nanofibers were used in this study:[1] nanofibers prepared by marginalizing the chloroform-solvated polymer environment with dichloromethane to a final v/v ratio of 1:7 $CHCl_3$:CH_2Cl_2 (referred to as the "mixed solvent");[2] nanofibers prepared from a solution of *p*-xylene. The mixed solvent presents a milder environment for the polymer with slower crystallization rates, while crystallization in *p*-xylene is highly accelerated due to poorer polymer solubility. Within each solvent family, we generated nanofibers made from both commercially available regioregular P3HT (Reike Metals, 15 000 MW, 93% regioregularity) and P3HT of high regioregularity (hrr) (98%) prepared by the Grignard metathesis (GRIM) polymerization of 2,5-dibromo-3-hexylthiophene, as reported by McCullough and co-workers.[44] A critical experimental issue for spectroscopic study of isolated nanofibers is to reach suitably dilute concentrations without compromising the nanofiber structure. To accomplish this, P3HT nanofiber suspensions were diluted in heptane (a marginal solvent for P3HT with high vapor pressure) in order to minimize fiber bunching (typically 10 μL of NFs in 1:7 chloroform/DCM to ≈0.75 mL of heptane). To prevent precipitation, 0.25 mL of the chloroform/DCM mixture was added to the heptane suspension for a final volume of about 1 mL. A small amount of the suspension of NFs in heptane was drop-cast on to a plasma cleaned glass coverslip, which gave a density of about five well-separated nanofibers in an area of ≈100 μm^2. All nanofibers were probed directly on glass with no host polymer (e.g., PMMA) matrix.

Isolated P3HT nanofibers were excited with a weakly focused (≈20 μm diameter spot size) pulsed diode laser (440 or 532 nm) set up in epi-illumination geometry with an average input intensity of about 1 kW/cm^2. The fluorescence was collected through the same objective and combination of dichroic mirror and long-pass filter (Omega Optical XF3082, 530 nm cut-on) which images almost exclusively the aggregate component of the PL spectrum.[24] The fluorescence was then imaged into two channels by a 50/50 neutral beam splitter, and a pair of linear analyzers, oriented in orthogonal directions to define detection

dx.doi.org/10.1021/jp308503u | J. Phys. Chem. C 2012, 116, 23803−23811

channels corresponding to parallel (H) and perpendicular (V) polarizations relative to the excitation polarization. Fluorescence photons in each channel were detected by separate avalanche photodiode detectors (APD, ID Quantique 400), whose output pulses were sorted via a high-precision router and input to the TCSPC module (PicoQuant PicoHarp300). While essentially the entire NF is illuminated in a particular experiment, the combination of magnification and spatial filtering (primarily by the spatial extent of the APDs), we detect only ≈500 nm segment of the NF photoluminescence in a TRPL run.

In conventional time-tagged-time resolved (T3R) single photon counting spectroscopy, fluorescence intensity trajectories are readily constructed by binning detected photon events by coarse (absolute) time in regular intervals or lifetime trajectories by sorting photon events by local (relative) arrival time within a given absolute time interval. The addition of a polarization tag allows us to access information about the time scales for depolarization in the nanofiber system by looking at the polarization contrast ratio, defined as $M(\tau) = (I_{para} - I_{perp})/(I_{para} + I_{perp})$ as a function of relative time, τ, following the excitation pulse, where para/perp can be explicitly defined relative to the nanofiber axis. In a typical measurement, two TCSPC (local arrival time) histograms are generated corresponding to the two polarization channels; the time-dependent polarization contrast parameter, $M(\tau)$, can be readily determined with a resolution that is limited ultimately by the time-to-digital converter (~4 ps) and over a dynamic range that is determined by the laser repetition rate (25−200 ns). The polarization contrast ratio as a function of relative detection time thus gives direct information on the equilibration time scale for intra- vs interchain excitations.

3. RESULTS AND DISCUSSION

3.1. Short Time PL Decay Behavior of P3HT Nanofibers: Effect of Molecular Weight and Regioregularity.

As we have previously reported,[8] single P3HT chains drop-cast from dilute chloroform solutions show reproducible single-exponential decay dynamics with a lifetime of ~600 ps. The emergence of short lifetime transients or long-time power law decay in thin films,[10,25] nanoparticles,[12] and nanofibers[23,24] are not seen in single chain luminescence and appear to be cooperative effects that are related to crystalline aggregates. In our previous work on wavelength-resolved photoluminescence of isolated nanofibers, we observed subtle differences in the PL spectra from nanofibers made from P3HT of different molecular weights and regioregularity suggestive of different intra- and interchain coupling. In this section, we examine the short-time luminescence of different nanofiber families to identify the role of intra- and interchain coupling on both relative amplitude and decay constant in the short and intermediate time regimes. In all cases, the nanofibers showed nonexponential short-time decay behavior, where the relative amplitude of the short-time component and decay rate increases nonlinearly with increasing pump power. Changes in the dispersion (reproducibility) of the decay parameter distributions depend sensitively on the nature of the P3HT and processing conditions, suggesting that varying degrees of structural heterogeneity exist within each family of nanofibers.

Figure 2 shows typical PL decay from two different nanofibers made from the mixed solvent using 15 kDa/93% rr-P3HT. In the 0−5 ns time range, the PL decay was biexponential with exponential decay parameters τ_1 (nominally

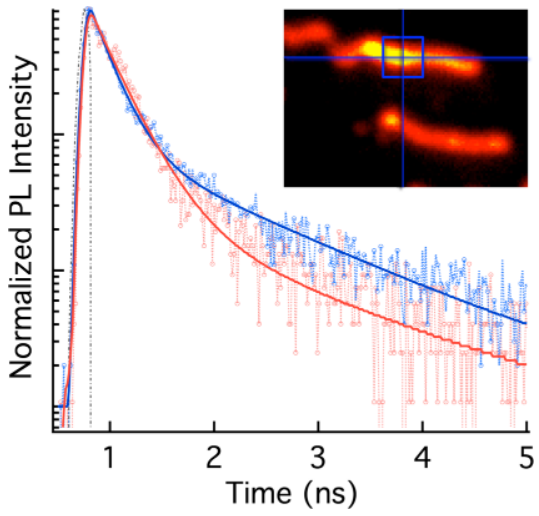

Figure 2. Typical short-time PL decay from two different P3HT nanofibers made from 15 kDa 93% rr-P3HT illustrating the heterogeneity in PL decay within a nanofiber family. The solid curves represent double-exponential fits to the TRPL decay curves for single P3HT NFs drop-cast on glass. The inset is a PL image of two extended nanofibers, with the blue box indicating the collection area of about 1 μm^2.

180 ps) and τ_2 (~1.5 ns). The τ_1 process is much faster than normal relaxed singlet exciton recombination and accounts for a surprisingly large fraction of the PL decay (>90%). We have observed a similar decay component in the PL from semicrystalline P3HT nanoparticles with typical relative amplitudes that vary from 75 to 95% depending on size and crystal fraction. Our hypothesis was that this short-time decay component derives from biexciton recombination: a cooperative effect between excitons on closely spaced adjacent chains in which the recombination of one exciton enhances the probability of the adjacent exciton recombination. As a cooperative two-exciton process, the amplitude (and decay rate) for this process should scale quadratically as a function of excited-state population.

Figure 3 shows the PL decay from the same nanofiber excited with 300 μW (blue) and 600 μW (red) average power. The inset shows the dependence of the prompt transient decay constant and amplitude (extracted from fitting the PL decay) from the same isolated nanofiber scanning excitation power.[a] The fit to τ_1 amplitude vs laser power shows a clear quadratic dependence, consistent with a biexciton decay process. The lifetime of this process decreases (decay rate increases) with increasing laser power, which is also consistent with a biexciton decay process, but because of signal-to-noise constraints (primarily due to low count rates at the lower laser powers), it is difficult to say definitively whether $1/\tau_1$ is actually quadratic. Decrease in the PL lifetime in P3HT films has recently been reported by Rumbles[26] and co-workers to result from exciton quenching due to intrinsic (dark) charge carriers in P3HT systems, with a number density estimated to be $\approx 10^{15}-10^{20}$ cm^{-3}. In an isolated nanofiber, if we assume a carrier density of $\sim 10^{16}$ cm^{-3}, then the number of dark carriers (per μm length) is of order unity and should not significantly affect the relaxation dynamics. Finally, as indicated on the main graph in Figure 4, the total PL count rate also shows a nonlinear increase with excitation power, consistent with a

dx.doi.org/10.1021/jp308503u | J. Phys. Chem. C 2012, 116, 23803−23811

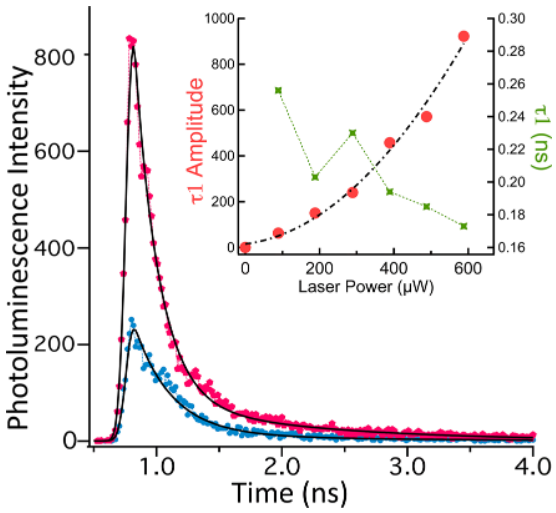

Figure 3. Power dependence of A_1 and τ_1. Main plot: TRPL decay curves from a single nanofiber excited with 300 μW (blue circles) and 600 μW (pink circles) and showing an approximately 4× increase in the emission intensity with 2× increase in excitation flux. Inset: amplitude of τ_1 (left axis) and lifetime (τ_1, right axis) vs input power, showing quadratic increase of amplitude and decrease in lifetime.

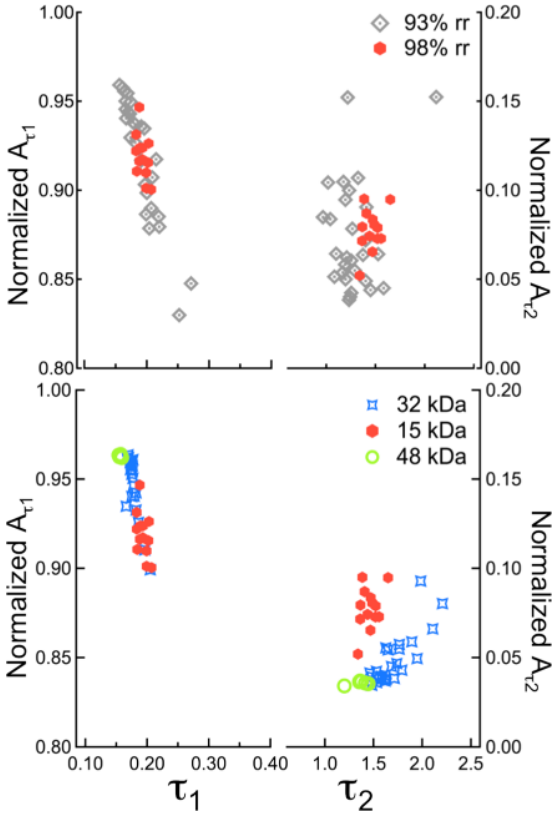

Figure 4. Comparison of fluorescence lifetime components and their respective normalized amplitudes from biexponential fits to the short-time regimes (<10 ns) of TRPL decay curves for single P3HT NFs drop-cast on glass. (a) shows these parameters for a collection of single NFs made with 14 kDa P3HT with 93% regioregularity (gray diamonds, PDI = 2) and 98% (red, PDI = 1.1). (b) is a similar plot comparing NFs made with 98% regioregular P3HT with MW = 14 kDa (red circles), 32 kDa (blue diamonds), and 48 kDa (green open circles).

biexciton decay process like amplified spontaneous emission, rather than a quenching process.

This assignment is useful in elucidating structural information from the short-time relaxation dynamics in crystalline P3HT nanofibers. Knoester[45] and Spano[46] have related inhomogeneous spectral broadening for individual chains in P3HT crystalline aggregates, showing that polymer chains within an aggregate should have identical transition frequencies (decreased inhomogeneous broadening) if the spatial correlation length significantly exceeds the conjugation length of the chains. Our hypothesis is that the effects of site heterogeneity also manifest as distributed kinetics in relaxation processes; thus, the dispersion of PL decay parameters for the associated spectral transitions should correlate with the degree of structural disorder within the aggregate.

Figure 4 shows the dispersion of PL decay parameters (amplitude and time constant) associated with the short time fluorescence from different NF subfamilies prepared from mixed solvent using P3HT with different regioregularity (top) and molecular weight (bottom). We extracted amplitudes (A_1, A_2) and time constants (τ_1, τ_2) from biexponential fits to the PL decay ($t \leq 5$ ns) and then generated correlation plots of the amplitudes (A_1, A_2) vs lifetimes (t_1, t_2). Figure 4a shows the effect of regioregularity for NFs of 93% and 98% regioregularity (both with 14 kDa MW). For the 93% rr P3HT, the nanofibers show significant dispersion (A_1 = 0.92 ± 0.034, τ_1 = 0.191 ± 0.027) in parameters associated with both PL decay components, while the dispersion in PL decay parameters from nanofibers prepared from the 98% rr P3HT is considerably smaller (A_1 = 0.91 ± 0.012, τ_1 = 0.193 ± 0.008). This analysis shows that regioregularity significantly impacts aggregate order in individual nanofibers.

Figure 4b shows the normalized A_1 vs τ_1 and A_2 vs τ_2 correlation plots for NFs assembled from 98% rr P3HT with 15, 32, and 48 kDa molecular weight. This analysis shows that the contribution (amplitude) of τ_1 (biexciton aggregate emission) to the total PL decay increases with increasing molecular weight, while τ_1 remains fairly constant. This molecular weight effect may also be (partly) responsible for the dispersion of A_1 among different regioregular P3HT nanofibers (Figure 4a) with the same average molecular weight, but with a larger polydispersity index (PDI = 2 vs 1.1 for orange circles). The two NF families (98% rr and 93% rr) have identical average values of τ_1 (τ_1 = 0.191) and A_1 (A_1 = 0.91) but with much larger variation in relative contribution of τ_1 (0.034 vs 0.012). Interestingly, the change in the regioregularity manifests in an increase in τ_2 (τ_2 = 1.46 ± 0.089 in 98% rr NFs and τ_2 = 1.28 ± 0.220 in 93% rr NFs), presumably as a result of increased intrachain order (effective conjugation length). The increase in the biexciton recombination rate with increasing molecular weight also reflects increase in intrachain order in the higher molecular weight polymer chains. This may also reflect the well-known solubility effect that causes fractionation,[20,47] in which the heaviest and most regioregular polymer chains will crystallize more readily under the same conditions as their lower MW and rr counterparts. The decreasing solubility of higher molecular weight polymer in the marginal solvent may encourage the chains to be more planar and therefore pack more closely, increasing the efficiency of biexciton recombination and manifesting as an increase in A_1 and slight decrease in t_1.

3.2. Solvent Effects on the Intra/Interchain Coupling.

Nanofibers formed from the chloroform−dichloromethane

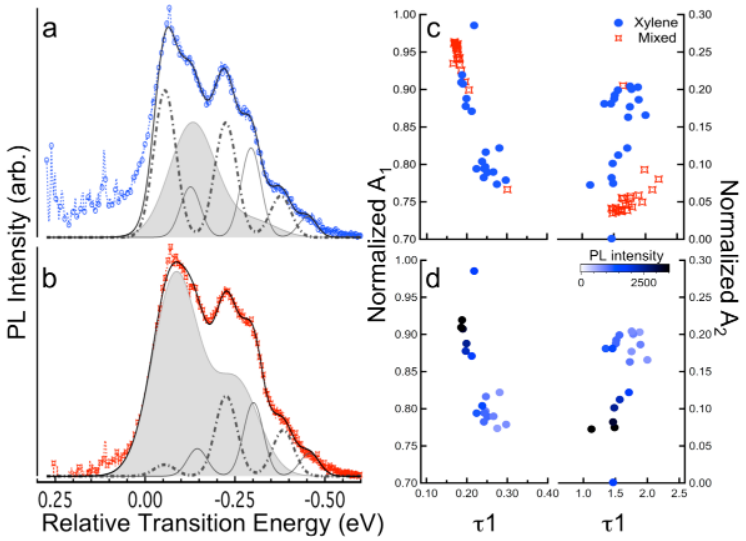

Figure 5. Representative photoluminescence spectra from single P3HT nanofibers made from xylene (a) and mixed (chloroform/DCM) solvent (b). The vibronic progressions that compose the model spectrum (black solid curve) are shown in gray, and the j-type sequence has been filled to illustrate the relative contribution. Amplitude/lifetime correlation plots for nanofibers made from each solvent are shown in (c). The PL intensity dependence of the correlation plot is color encoded in (d) for the xylene-formed nanofibers.

solvent mixture have been shown by X-ray diffraction to have a high degree of long-range order in the interchain (010 π-stacking) direction.[20] Conversely, NFs formed from *p*-xylene, a bad solvent for P3HT, show characteristic XRD signatures of chain packing defects. This is also reflected in the photoluminescence spectra from single nanofibers formed from xylene (a) and the mixed solvent system (b) with 532 nm excitation also shown in Figure 5. As in our earlier report,[24] the PL spectra were modeled as a sum of three different vibronic progressions. In contrast with NFs made from the mixed solvent, which show two H-like spectral components and a single J-like species (Figure 5b), NFs made from xylene show one *J*-like species, one H-component, and a third component which is ambiguous (with 0−0/0−1 intensity ratios for NFs in this family forming a distribution with a mean value of around 1) (Figure 5a). We hypothesize the presence of the "uncoupled" polymer chain vibronic sequence (with I_{0-0}/I_{0-1} ~1) in the xylene-formed NFs to be a spectral signature of low degrees of spatial correlation along the π-stack axis. Furthermore, in the absence of proper interchain communication, there seems to be an enhancement of the intrachain coupling strength (a 3-fold increase in I_{0-0}/I_{0-1} for the j-type sequence, Figure 5a, filled) when compared to the analogous sequence in the mixed solvent Nfs (Figure 5b, filled). This is perhaps an indication that the inter/intrachain exciton population equilibrium may favor the intrachain states in the absence of good spatial correlation along the π-stack axis.

Figure 5c shows amplitude/lifetime correlation plots for the short-time decay components for nanofibers of the same P3HT (32 kDa, 98% rr) formed from xylene and from the mixed solvent system. The distribution of t_1 amplitudes for the xylene family is clearly bimodal with some nanofibers showing decay dynamics similar to those formed from the mixed solvent system and a well-separated subpopulation of NFs showing very low rates of biexciton recombination. Figure 5d shows that the total PL intensity is proportional to the amplitude of τ_1, further illustrating that this biexciton amplified spontaneous emission process dominates the relaxation process.

3.3. Polarization Evolution in Single P3HT Nanofibers.

Cooperative photophysical effects in crystalline P3HT nanostructures derive from interactions between different cofacially aligned thiophene rings in a π-stack (H-type coupling) or between adjacent planar segments of the same polymer chain (J-type coupling). Because the directions of these interactions are almost completely orthogonal in the quasi-2D nanofibers, photophysical properties associated with inter- and intrachain recombination events are anticipated to be highly polarized in orthogonal directions. However, this information is obscured in NF ensembles, thin films, and nanoparticles because of the random orientation of the crystal growth (b) axis. For isolated NFs, time- and polarization-resolved photoluminescence measurements provide a means to directly probe these interactions in the NF frame—either parallel (b polarized) or perpendicular (a−c polarized) to the nanofiber axis. In these experiments, different nanofibers were selected with long axes oriented parallel or perpendicular to the linear excitation polarization; from the polarization "tag" attached to each photon detection event, we generated the polarization contrast parameter, $M(\tau) = (n_{ac} - n_b)/(n_{ac} + n_b)$, where $n_{ac/b}$ is the number of detected photons in a polarization perpendicular/parallel (to the *nanofiber long axis*) channel at relative time, τ (ps).

Figure 6 (lower) shows the picosecond-resolved polarization anisotropy parameter, $M(\tau)$, for nanofibers formed from *p*-xylene (a) and mixed solvent (b) for long axes oriented parallel (blue) and perpendicular (red) to the excitation polarization. Here, a positive value of M corresponds to an anisotropy *perpendicular (transverse)* to the nanofiber axis (intrachain excitons), while negative anisotropy values correspond to emission primarily parallel to the nanofiber axis. For the xylene-formed nanofibers with *b*-axis orientation perpendicular to the excitation polarization (Figure 6a, red), we observed a strong positive anisotropy ($M \approx +0.6$) at early times following the excitation pulse, which decays to a negative ($M \approx -0.4$) anisotropy on a time scale of ≈300 ps. This indicates that a significant fraction of the PL decay (for transverse excitation) is polarized along the nanofiber axis (i.e., has significant interchain

dx.doi.org/10.1021/jp308503u | J. Phys. Chem. C 2012, 116, 23803−23811

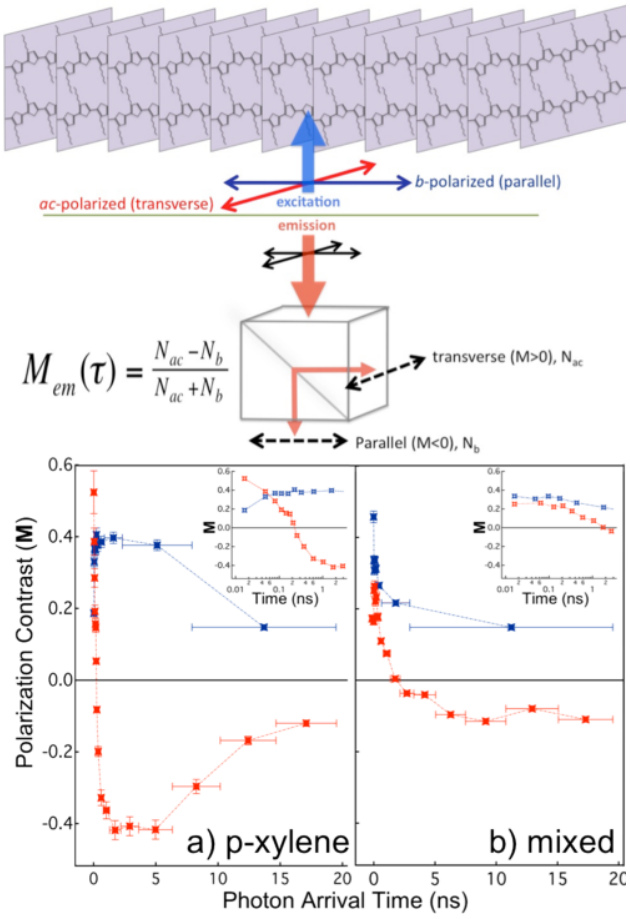

Figure 6. Time-resolved polarization contrast parameter $M(\tau)$ vs photon arrival time for single nanofibers made from *p*-xylene (a) and the chloroform/DCM solvent mixture (b). The red traces represent $M(t)$ when excitation polarization is oriented transverse to the nanofiber π-stack axis, and blue traces are the same under parallel-polarized excitation. The insets are expanded views of the short time dynamics designed to highlight the difference in depolarization times between the two samples.

character). For excitation polarization parallel to the nanofiber long axis (Figure 6b, blue), the polarization anisotropy is also positive but is essentially constant over the 0.1−10 ns time interval.

Parallel (Figure 6b, blue) and perpendicular (Figure 6b,red) excitation of nanofibers formed in the marginal chloroform/DCM solvent mixture reveals qualitative similarities to their xylene-formed counterparts, with clear differences in the magnitudes of M and time scales associated with depolarization. The maximum value of M for the mixed solvent NF is only +0.3, and the minimum is even shallower at $M = -0.15$. Examination of the inset plots in Figure 6, which show the short-time behavior on an expanded (log) time scale, reveals that the initial depolarization time for $M(\tau)$ (in the red curves) is an order of magnitude longer for the mixed solvent fibers, which depolarize over the course of more than 1 ns, compared to about ∼180 ps in the xylene fibers. When excited with parallel polarization to the nanofiber long axis, the emission is again always positive, although the anisotropy decays quickly, rather than remaining constant over the 10 ns range.

The picture that has emerged from this study is that both intra- and interchain excitons are formed with either transverse or parallel excitation polarization with an initial equilibrium established on a time scale shorter than our instrumental resolution (4 ps). For transverse excitation, more efficient production of intrachain excitons leads to amplified spontaneous emission (τ_1 process) that depletes the population of intrachain excitons on a time scale of ≈300 ps, giving rise to the strong short-time positive polarization anisotropy (and subsequent rapid decay). The excitations that remain are primarily interchain excitons that decay on a much longer time scale, and are associated with a negative anisotropy. Conversely, for parallel excitation, relatively little ASE occurs, and the time-dependent polarization anisotropy reflects the equilibrium (steady state) populations of inter and intra chain excitons. The significant compression of the magnitude of $M(\tau)$ for the mixed solvent fibers (compared to the xylene fibers) is thought to be a result of better interchain order, which allows more excitonic population of the interchain states. More detailed studies on the time evolution of polarization contrast in individual nanofibers will be reported elsewhere. Altogether, we find that $M(t)$ for the nanofibers formed under milder conditions (marginal mixed solvent) shows much closer competition for population of the inter- vs intrachain states. This competition is heavily affected by solvent quality, in that decreasing the solvent quality generally decreases in the long-range interchain order.

3.4. Long Time Decay Dynamics in NFs: Dynamics of Charge-Separated States. The inter- and intrachain processes that manifest as distinct vibronic species in the emission spectrum also have interesting manifestations in the long-time PL decay dynamics. In the 5−100 ns time regime, the photoluminescence derives from exciton dissociation followed by polaron diffusion and ultimately recombination via tunneling.[25] As in thin films[25,30,49] or nanoparticles,[12] the PL decay in this time regime follows a power law ($I[t] \approx At^{-[1+\mu]}$), where $(1 + \mu)$ is slope of the log PL count rate vs log[t] plot. In the model proposed by Silva and co-workers,[25] when polaron pairs recombine via tunneling, the power law exponent, μ, is inversely proportional to the mean electron−hole radius, R. For trapped charge carriers, the recombination rate will reflect the lifetime (depth) of the trap state.

Figure 7 shows three representative PL decay traces from different individual nanofibers in the long time (10−100 ns) regime, where we have identified three different distinct behaviors: single power law (top, blue), double power (middle, red), and a single power law followed by an apparent dc offset which is the subpower law region (bottom, green). The onset time and initial decay dynamics of the power law region (≈ 5−20 ns) are similar for all nanofibers studied, while the slope (power law exponent) and relative contribution can vary significantly. In thin films and nanoparticles, the observation of power law decay is the signature of exciton dissociation, followed by long-time carrier diffusion and polaron-pair recombination.[38,48−51] The appearance of a double- or subpower law behavior is not observed in thin films or nanoparticles and thus appears to be unique to P3HT nanofibers.

The vertical lines indicate the region of the decay (≈ 4−15 ns) used to identify the primary power law exponent μ_1. The right panel shows histograms of μ_1 for three different P3HT NF families: (A) 14K MW; (B) 93% rr, 14K MW; (C) 98% rr, and 32K MW, 98% rr. These results show clearly that the mean power law exponent is to within experimental uncertainty independent of molecular weight for given regioregularity and

dx.doi.org/10.1021/jp308503u | J. Phys. Chem. C 2012, 116, 23803−23811

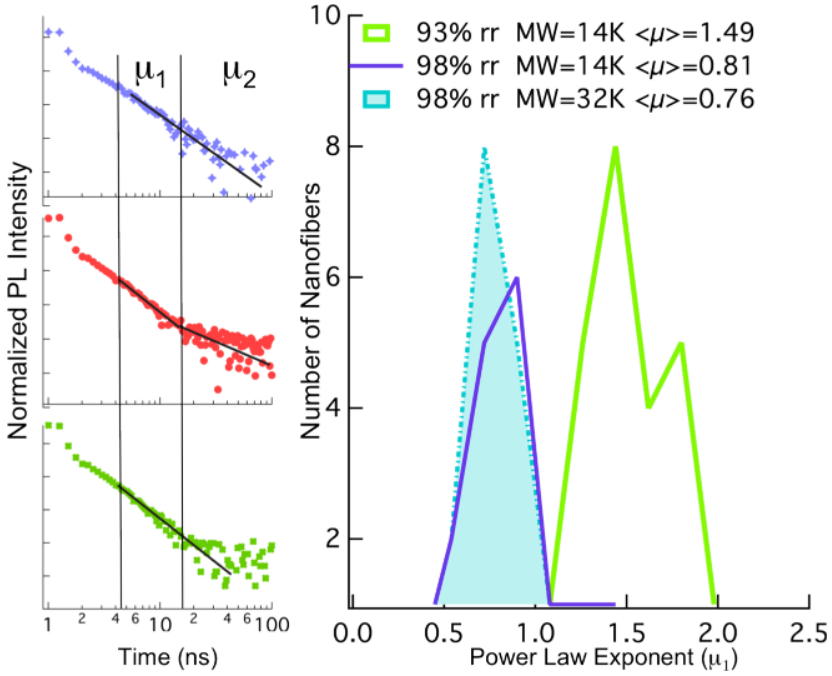

Figure 7. Left: three typical decay profiles from single nanofibers showing single power law (blue), double power law (red), and power law plus sub power law behavior (green). Right: histogram of power law exponents from first power law region (μ_1, indicated on right) of PL decay from three families of nanofibers made from 14 kDa P3HT with 93% and 98% regioregularity and 32 kDa P3HT with 98% regioregularity.

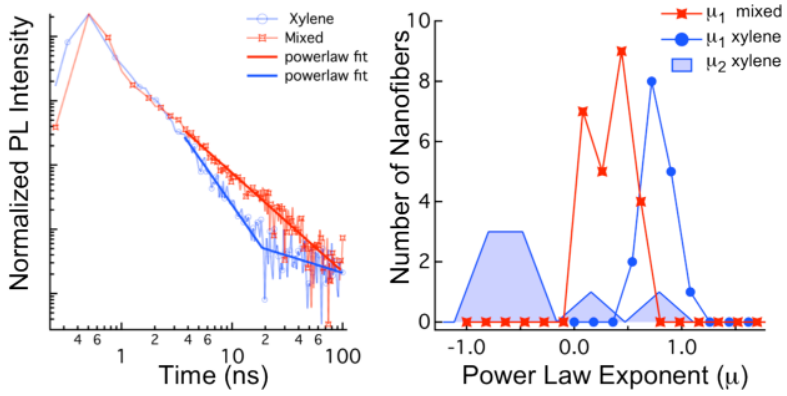

Figure 8. Decay profiles and power law fits for 32 kDa 98% rr P3HT nanofibers formed from xylene (blue) and chloroform/DCM (red) and histograms of power law exponents obtained from those fits (right).

increases significantly with decreasing regioregularity for given molecular weight. In all three cases, μ_1 is significantly larger than the reported thin-film value of $\mu = 0.54$, suggesting a smaller mean electron−hole distance in nanofibers; the large (≈2×) increase in μ_1 with decrease in regioregularity (which affects both intra- and interchain order) suggests an even tighter polaron−pair distance in the lower rr NFs.

Figure 8 shows representative long time PL decay dynamics from 32 kDa P3HT nanofibers made from xylene and mixed (chloroform/DCM) solvent. While NFs made from the mixed solvent show exclusively single power law dynamics, NFs made from *p*-xylene showed a double or subpower law behavior. We identified a second power law exponent, μ_2, in the time range of ≈20−100 ns, and the distribution of μ_2 values for NFs made from *p*-xylene is shown as a filled histogram in Figure 8b. Indeed, a large fraction of NFs from the *p*-xylene family have values of μ_2 that are negative; such decay behavior cannot be explained in the context of a dissociation−tunneling recombination model since μ must be a ratio of two positive numbers.[25] As seen by the distribution of power law exponents obtained from the different NF families, all power law exponents from the mixed solvent NFs have values intermediate to the two distributions μ_1 and μ_2 from the xylene-formed nanofibers. In the context of the solvent effects (and associated differences in chain packing defects), and the observed short-time polarization analysis, the subpower law behavior appears to derive from lamellar packing defects which simultaneously weaken interchain coupling and act as charge traps. It is also tempting to speculate that the enhancement of μ_1 (relative to the mean power law exponent for the mixed solvent) derives from an increase in intrachain tunneling as a response to the unavailable interchain pathway in the poorly packed nanofibers. Although the process of charge separation itself scrambles the polarization signature of these events, the combination of regioregularity and solvent effects (and the absence of a molecular weight effect) makes this assignment reasonable.

dx.doi.org/10.1021/jp308503u | *J. Phys. Chem. C* 2012, 116, 23803−23811

4. SUMMARY AND CONCLUSIONS

The time-resolved photoluminescence studies on isolated P3HT nanofibers presented here have enabled us to identify three distinct time domains associated with different recombination processes in crystalline P3HT nanostructures. The first two occur within the first 5 ns and are well described by exponential rate laws consistent with biexciton and single-exciton radiative decay processes, while the long time dynamics follow power law decays associated with charge-separation and polaron-pair recombination. Biexciton aggregate emission in the nanofiber accounts for more than 90% of PL emission, with an average time constant of ≈180 ps. The quantitative dependence on the amplitude and decay rate of this PL component was observed to be dependent on both regioregularity and molecular weight, indicating a delicate sensitivity to aggregate order and structural coherence. The relaxed singlet exciton decay, occurring on a time scale of ≈1.5 ns, is an intrachain species affected by the regioregularity and planarity (as indicated by the correlation with J-type spectral intensity) of the polymer chains in an aggregate. Roughly 1% of the PL decay is contained within the 5−100 ns time regime and follows a combination of power law, bilinear power law, or subpower law decay depending on the nature of the P3HT used in the nanofiber preparation or solvent processing conditions. There is sufficient evidence that charge separation processes occur along chains as well as between chains, producing the rate constants that describe the beginning and end power law behavior, respectively. The correlation between the subpower law behavior seen at very long time scales and the low biexciton recombination rates at very short times bolsters the hypothesis that there are deeper and more frequently occurring charge traps in the interchain direction.

We have identified the short-time PL decay component as a biexciton recombination process involving intrachain excitons, which appears as an amplified spontaneous emission (ASE) process between adjacent chains in an aggregate. Perhaps somewhat ironically, the implication is that the observed biexciton decay—which competes directly with exciton dissociation—is most efficient in the same well-ordered stacks of polymer chains that are also expected to efficiently separate and transport charges. Thus, it appears that increasing the structural order in this system also increases the rate of biexciton annihilation, which competes directly with charge separation. This presents an interesting challenge when using polythiophenes as photovoltaic materials, since structural defects that inhibit the biexciton process tend also to inhibit charge transfer between polymer chains. Finding a way to inhibit the amplified spontaneous emission, while maintaining charge separation and transport efficiencies in crystalline nanofibers will prove important to maximizing their performance in photovoltaic active layers.

AUTHOR INFORMATION

Corresponding Author

*E-mail: mdbarnes@chem.umass.edu.

Notes

The authors declare no competing financial interest.

ACKNOWLEDGMENTS

J.A.L. (time-resolved measurements) acknowledges support from the Energy Frontier Research Center funded by the U.S. Department of Energy, Office of Science, Office of Basic Energy Sciences, under Award DE-SC0001087. M.B. (PL spectral measurements) acknowledges support from NSF MRSEC (DMR-0820506). A.M. and M.D.B. acknowledge support from US Department of Energy (Program Manager: Larry Rahn, DE-FG02-05ER15695). The authors acknowledge Feng Liu and Emily Pentzer for synthesis of the highly regioregular P3HT used in these measurements and Sunzida Ferdous and Felicia Bokel for some of the nanofiber preparations. J.A.L. thanks Paul Homnick and Jonathan Tinkham for helpful conversations.

ADDITIONAL NOTE

[a]We used a variable neutral density filter to scan the excitation power which avoids potential artifacts in the decay profile associated with pulse distortions with increasing drive current on the pulsed diode laser head.

REFERENCES

(1) Hoppe, H.; Sariciftci, N. S. *J. Mater. Res.* **2004**, *19*, 1924−1945.
(2) Benanti, T. L.; Venkataraman, D. *Photosynth. Res.* **2006**, *87*, 73−81.
(3) Thompson, B. C.; Frechet, J. M. J. *Angew. Chem., Int. Ed.* **2008**, *47*, 58−77.
(4) Peet, J.; Heeger, A. J.; Bazan, G. C. *Acc. Chem. Res.* **2009**, *42*, 1700−1708.
(5) Po, R.; Maggini, M.; Camaioni, N. *J. Phys. Chem. C* **2010**, *114*, 695−706.
(6) Moule, A. J.; Meerholz, K. *Adv. Mater.* **2008**, *20*, 240−245.
(7) Venkataraman, D.; Yurt, S.; Venkatraman, B. H.; Gavvalapalli, N. *J. Phys. Chem. Lett.* **2010**, *1*, 947−958.
(8) Labastide, J. A.; Baghgar, M.; Dujovne, I.; Yang, Y. P.; Dinsmore, A. D.; Sumpter, B. G.; Venkataraman, D.; Barnes, M. D. *J. Phys. Chem. Lett.* **2011**, *2*, 3085−3091.
(9) Paquin, F.; Latini, G.; Sakowicz, M.; Karsenti, P.-L.; Wang, L.; Beljonne, D.; Stingelin, N.; Silva, C. *Phys. Rev. Lett.* **2011**, *106*, 197401.
(10) Banerji, N.; Cowan, S.; Vauthey, E.; Heeger, A. J. *J. Phys. Chem. C* **2011**, *115*, 9726−9739.
(11) Hukic-Markosian, G.; Basel, T.; Singh, S.; Vardeny, Z. V.; Li, S.; Laird, D. *Appl. Phys. Lett.* **2012**, 100.
(12) Labastide, J. A.; Baghgar, M.; Dujovne, I.; Venkatraman, B. H.; Ramsdell, D. C.; Venkataraman, D.; Barnes, M. D. *J. Phys. Chem. Lett.* **2011**, *2*, 2089−2093.
(13) Hu, Z. J.; Tenery, D.; Bonner, M. S.; Gesquiere, A. J. *J. Lumin.* **2010**, *130*, 771−780.
(14) Bai, X.; Holdcroft, S. *Macromolecules* **1993**, *26*, 4457−4460.
(15) Theander, M.; Anderson, M. R.; Inganas, O. *Synth. Met.* **1999**, *101*, 331−332.
(16) Ruseckas, A.; Namdas, E. B.; Ganguly, T.; Theander, M.; Svensson, M.; Andersson, M. R.; Inganas, O.; Sundstrom, V. *J. Phys. Chem. B* **2001**, *105*, 7624−7631.
(17) Jiang, X. M.; Osterbacka, R.; Korovyanko, O.; An, C. P.; Horovitz, B.; Janssen, R. A. J.; Vardeny, Z. V. *Adv. Funct. Mater.* **2002**, *12*, 587−597.
(18) Briseno, A. L.; Mannsfeld, S. C. B.; Jenekhe, S. A.; Bao, Z.; Xia, Y. N. *Mater. Today* **2008**, *11*, 38−47.
(19) Newbloom, G. M.; Kim, F. S.; Jenekhe, S. A.; Pozzo, D. C. *Macromolecules* **2011**, *44*, 3801−3809.
(20) Roehling, J. D.; Arslan, I.; Moule, A. J. *J. Mater. Chem.* **2012**, *22*, 2498−2506.
(21) Kim, T.; Im, J. H.; Choi, H. S.; Yang, S. J.; Kim, S. W.; Park, C. R. *J. Mater. Chem.* **2011**, *21*, 14231−14239.
(22) Lee, S. H.; Park, D. H.; Kim, K.; Joo, J.; Kim, D. C.; Kim, H. J.; Kim, J. *Appl. Phys. Lett.* **2007**, 91.
(23) Niles, E. T.; Roehling, J. D.; Yamagata, H.; Wise, A. J.; Spano, F. C.; Moule, A. J.; Grey, J. K. *J. Phys. Chem. Lett.* **2012**, *3*, 259−263.

(24) Baghgar, M.; Labastide, J. A.; Bokel, F.; Pentzer, E.; Barnes, A. M.; Hayward, R.; Emrick, T.; Barnes, M. D. *J. Phys. Chem. Lett.* **2012**, in press.
(25) Paquin, F.; Latini, G.; Sakowicz, M.; Karsenti, P. L.; Wang, L. J.; Beljonne, D.; Stingelin, N.; Silva, C. *Phys. Rev. Lett.* **2011**, 106.
(26) Reid, O. G.; Malik, J. A. N.; Latini, G.; Dayal, S.; Kopidakis, N.; Silva, C.; Stingelin, N.; Rumbles, G. *J. Polym. Sci., Polym. Phys.* **2012**, *50*, 27−37.
(27) Dang, M. T.; Hirsch, L.; Wantz, G. *Adv. Mater.* **2011**, *23*, 3597−3602.
(28) Busby, E.; Carroll, E. C.; Chinn, E. M.; Chang, L. L.; Moule, A. J.; Larsen, D. S. *J. Phys. Chem. Lett.* **2011**, *2*, 2764−2769.
(29) Busby, E.; Rochester, C. W.; Moule, A. J.; Larsen, D. S. *Chem. Phys. Lett.* **2011**, *513*, 77−83.
(30) Jiang, X. M.; Osterbacka, R.; An, C. P.; Vardeny, Z. V. *Synth. Met.* **2003**, *137*, 1465−1468.
(31) Kim, Y.; Cook, S.; Kirkpatrick, J.; Nelson, J.; Durrant, J. R.; Bradley, D. D. C.; Giles, M.; Heeney, M.; Hamilton, R.; McCulloch, I. *J. Phys. Chem. C* **2007**, *111*, 8137−8141.
(32) Keivanidis, P. E.; Clarke, T. M.; Lilliu, S.; Agostinelli, T.; Macdonald, J. E.; Durrant, J. R.; Bradley, D. D. C.; Nelson, J. *J. Phys. Chem. Lett.* **2010**, *1*, 734−738.
(33) Brown, P. J.; Thomas, D. S.; Kohler, A.; Wilson, J. S.; Kim, J. S.; Ramsdale, C. M.; Sirringhaus, H.; Friend, R. H. *Phys. Rev. B* **2003**, 67.
(34) Westenhoff, S.; Daniel, C.; Friend, R. H.; Silva, C.; Sundstrom, V.; Yartsev, A. *J. Chem. Phys.* **2005**, 122.
(35) Ho, P. K. H.; Chua, L. L.; Dipankar, M.; Gao, X. Y.; Qi, D. C.; Wee, A. T. S.; Chang, J. F.; Friend, R. H. *Adv. Mater.* **2007**, *19*, 215−219.
(36) Clark, J.; Silva, C.; Friend, R. H.; Spano, F. C. *Phys. Rev. Lett.* **2007**, 98.
(37) Clark, J.; Chang, J. F.; Spano, F. C.; Friend, R. H.; Silva, C. *Appl. Phys. Lett.* **2009**, 94.
(38) Ferguson, A. J.; Kopidakis, N.; Shaheen, S. E.; Rumbles, G. *J. Phys. Chem. C* **2011**, *115*, 23134−23148.
(39) Schenning, A. P. H. J.; Meijer, E. W. *Chem. Commun.* **2005**, 3245−3258.
(40) Berson, S.; De Bettignies, R.; Bailly, S.; Guillerez, S. *Adv. Funct. Mater.* **2007**, *17*, 1377−1384.
(41) Shimomura, T.; Takahashi, T.; Ichimura, Y.; Nakagawa, S.; Noguchi, K.; Heike, S.; Hashizume, T. *Phys. Rev. B* **2011**, 83.
(42) Brinkmann, M.; Rannou, P. *Macromolecules* **2009**, *42*, 1125−1130.
(43) Yamagata, H.; Spano, F. C. *J. Chem. Phys.* **2012**, *136*, 14.
(44) Loewe, R. S.; Khersonsky, S. M.; McCullough, R. D. *Adv. Mater.* **1999**, *11*, 250−253.
(45) Knoester, J. *J. Chem. Phys.* **1993**, *99*, 8466−8479.
(46) Spano, F. C. *Chem. Phys.* **2006**, *325*, 22−35.
(47) Do, K.; Huang, D. M.; Faller, R.; Moule, A. J. *Phys. Chem. Chem. Phys.* **2010**, *12*, 14735−14739.
(48) Vardeny, Z.; Grahn, H. T.; Heeger, A. J.; Wudl, F. *Synth. Met.* **1989**, *28*, C299−C304.
(49) Hess, B. C.; Shinar, J.; Ni, Q. X.; Vardeny, Z.; Wudl, F. *Synth. Met.* **1989**, *28*, C365−C370.
(50) Ai, X.; Beard, M. C.; Knutsen, K. P.; Shaheen, S. E.; Rumbles, G.; Ellingson, R. J. *J. Phys. Chem. B* **2006**, *110*, 25462−25471.
(51) Ferguson, A. J.; Kopidakis, N.; Shaheen, S. E.; Rumbles, G. *J. Phys. Chem. C* **2008**, *112*, 9865−9871.